The American Journal of Human Genetics, Volume *101*

Supplemental Data

Mutations in *TUBB4B* Cause a Distinctive Sensorineural Disease

Romain Luscan, Sabrina Mechaussier, Antoine Paul, Guoling Tian, Xavier Gérard, Sabine Defoort-Dellhemmes, Natalie Loundon, Isabelle Audo, Sophie Bonnin, Jean-François LeGargasson, Julien Dumont, Nicolas Goudin, Meriem Garfa-Traoré, Marc Bras, Aurore Pouliet, Bettina Bessières, Nathalie Boddaert, José-Alain Sahel, Stanislas Lyonnet, Josseline Kaplan, Nicholas J. Cowan, Jean-Michel Rozet, Sandrine Marlin, and Isabelle Perrault

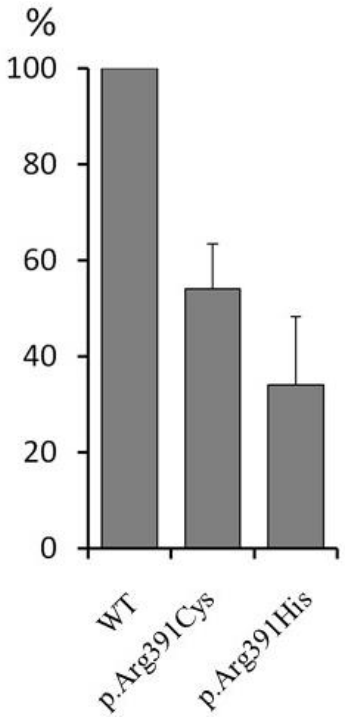

Figure S1. Quantification of ^{35}S-methionine-labeled TUBB4B wild type, p.Arg391Cys and p.Arg391His αβ-tubulin heterodimers produced by in vitro transcription/translation.

Quantification of relative yields of ^{35}S-methionine-labeled TUBB4B wild type (WT), p.Arg391Cys and p.Arg391His αβ-tubulin heterodimers produced by in vitro transcription/translation for 90 mins and chased for a further 30 mins with added depolymerized brain tubulin (see Figure 2B). The yield of WT αβ-tubulin heterodimers is taken as 100%. Data are presented as mean ± SD from six independent reactions, in each case measured using a phosphoimager.

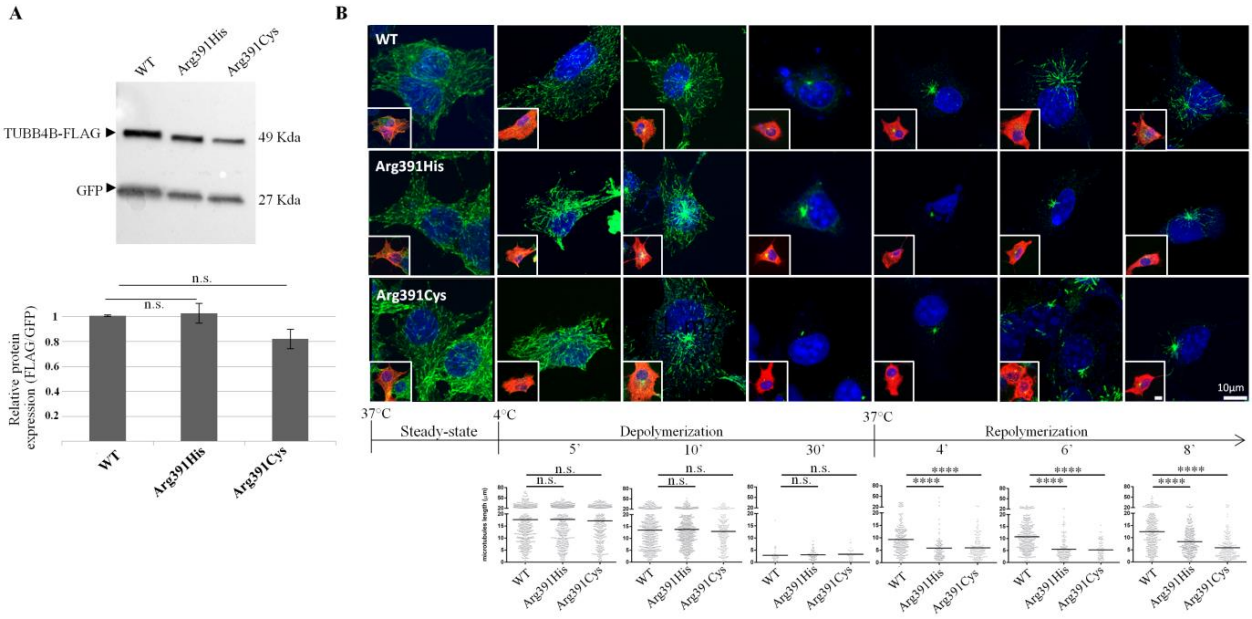

Figure S2. Overexpression of TUBB4B p.Arg391Cys and p.Arg391His affects the polymerization dynamics of COS7 microtubules.

(**A**) Western blot (upper panel) and computed-densitometry (lower panel) analysis of wild-type and mutant FLAG-tagged TUBB4B relative to GFP. COS7 cells were co-transfected with wild-type or mutant FLAG-tagged TUBB4B plasmids (800 ng) and the pCAGGS-GFP plasmid (200 ng; Clontech, California, USA) using the FuGene HD transfection reagent according to the manufacturer's protocol (Promega, Charbonnières-les-Bains, France). After 48 hours, GFP-expressing cells were sorted on a Sony SH800 cell sorter (Sony Biotechnology, San Jose, CA, USA). 50 µg of total protein prepared using RIPA lysis buffer (Life Technologies ThermoFisher Scientific) was resolved on a Mini-ProteanTGX Stain Free 4-20% gel according to the supplier's recommendations (BioRad, Marne la Coquette, France). Proteins were transferred to a PVDF membrane using a RTA transfer kit (BioRad) which was probed with the following primary antibodies: Monoclonal ANTI-FLAG® M2 antibody (Sigma Aldrich, Missouri USA); anti-GFP from mouse $IgG_1\kappa$ (clones 7.1 and 13.1) (Sigma Aldrich) and goat anti-mouse IgG-HRP and goat anti-rabbit HRP secondary antibodies (2 mg/mL, 1:10,000, Abcam, Paris, France). Blots were developed using the Clarity Western ECL and ChemiDoc XRS+ Imaging System (BioRad) and images were acquired and analyzed with Image Lab Software 3.0.1 build 18 (BioRad). The abundance of FLAG relative to GFP was estimated by densitometry using Image Lab Software 3.0.1 build 18. Values are means ± SD of densities from three independent transfection experiments. A t-Student test was used to compare the abundance of FLAG in the different experiments.

(B) Appearance and length of MTs. COS7 cells were transfected with wild-type or mutant FLAG-tagged TUBB4B plasmids as described in (A). After 48 hours, cells were fixed in ice-cold methanol (5 minutes at −20 °C) without further treatment (steady-state MT lattice) or after having been maintained on ice for 5, 10 and 30 min. (MT depolymerization) or for 30 min. prior to incubation at 37°C (MT repolymerization) for 4, 6 and 8 min., respectively. Fixed cells were permeabilized (1 hour, room temperature) and immunostained using mouse Anti-EB1 (1:200, overnight, 4°C, BD Biosciences, Le-Pont-De-Claix, France) and rabbit anti-FLAG (1:2000, overnight, 4°C; Sigma Aldrich) primary antibodies, and alexa fluor 488 donkey anti-mouse or alexa fluor 568 donkey anti-rabbit secondary antibodies (1:1000, 1 hour 37°C, Life Technologies ThermoFisher Scientific). A mounting medium containing 4′,6-diamidino-2-phenylindole (DAPI) (Prolong Gold, Life Technologies ThermoFisher Scientific) was used to label nuclei. Immunofluorescence images were obtained using a Spinning Disk Zeiss microscope (Zeiss, Oberkochen, Germany). Final images were generated using ImageJ (National Institutes of Health, Bethesda, MA, USA). Below each row of images, the individual distance of EB1 relative to the centrosome (determined using Icy software) is plotted as a dot, with the mean distance represented by a horizontal line. Statistical analyses were carried out by analysis of variance (ANOVA) and the PLSD Fisher test. ****: p-value < 0.0001. ; n.s.: non-significant p-value ≥ 0.5.

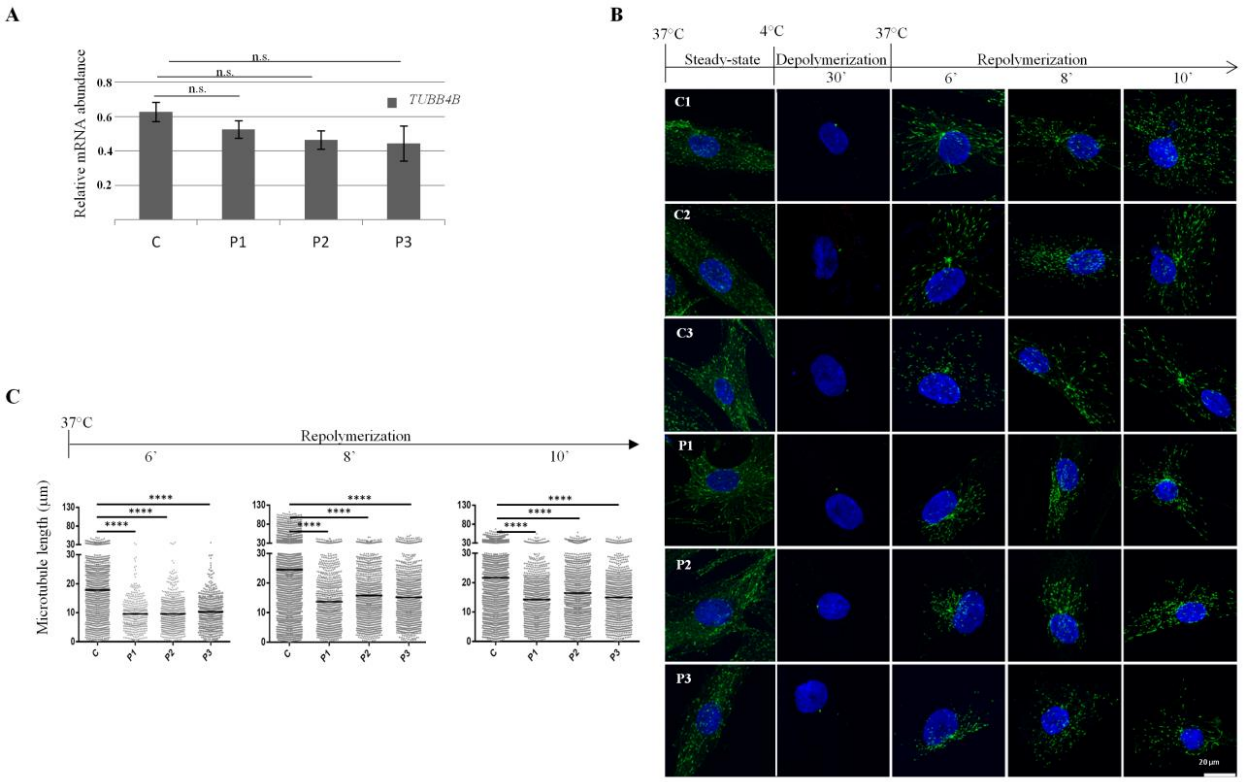

Figure S3. *TUBB4B* c.1172G>A and c.1171C>T mutations affect MT polymerization dynamics in patient fibroblasts.

(**A**) Relative abundance of *TUBB4B* mRNA in control (C) and affected patient-derived (P1, P2, P3) skin fibroblasts. *TUBB4B mRNA* abundance was measured from skin fibroblast RNA as described previously.[1] The *TUBB4B* cDNA was amplified as a 57 bp fragment using exonic primers: (forward, 5'-3') ggcccttcgggcagatctt and (reverse, 5'-3') cagcaccactctgaccgaaa. *B2M* (NM_004048.2), *HPRT1* (NM_000194), *RPLP0* (NM_001002.3) mRNAs and the *ALB* (NM_000477) gene were used to normalize the data and to control for potential contamination of cDNAs by genomic DNA. Primer sequences are available elsewhere[1]. The quantitative data are the means ± Standard Deviation (SD) of three experimental replicates and these are presented as ratios among values for individual mRNAs. The significance of variations among samples was determined using a Mann-Whitney statistic test. The graph shows no statistically significant reduction in *TUBB4B* mRNA abundance in affected individuals compared to controls C1, C2, C3 (regrouped in C). Data are presented as mean ± SEM. n.s.: non-significant.

(**B**) Appearance of steady-state, depolymerizing and repolymerizing microtubules in fibroblasts from control (C1, C2, C3) and affected (P1, P2, P3) individuals. Fibroblasts were directly fixed in ice-cold methanol (5 min. at −20 °C; steady-state MT lattice), maintained on ice for 30 min. (complete MT depolymerization) and fixed, or maintained on ice for 30 min. and incubated at 37°C (MT repolymerization) for 6, 8 or 10 min. and fixed. Fixed cells were permeabilized (1 hour, room temperature) and stained using a mouse Anti-EB1 primary antibody (1:200, overnight, 4°C; BD Biosciences) and an Alexa-Fluor 488– conjugated goat anti-mouse IgG (1:1,000; 1 hour, room temperature; Life Technologies ThermoFisher Scientific). A mounting medium containing DAPI (Prolong Gold, Life Technologies ThermoFisher Scientific) was used to label nuclei. Immunofluorescence images were obtained using a Spinning Disk Zeiss microscope (Zeiss). The final images were generated using ImageJ (National Institutes of Health, Bethesda, MA).

(**C**) The individual distance of EB1 relative to the centrosome determined using Icy software is plotted as a dot, with the mean distance represented by a horizontal line. Statistical analyses were carried out by analysis of variance (ANOVA) and the PLSD Fisher test. ****: p-value < 0.0001; n.s.: non-significant p-value ≥ 0.5. The control value C is the mean of values from C1, C2 and C3. ****: p-value < 0.0001.

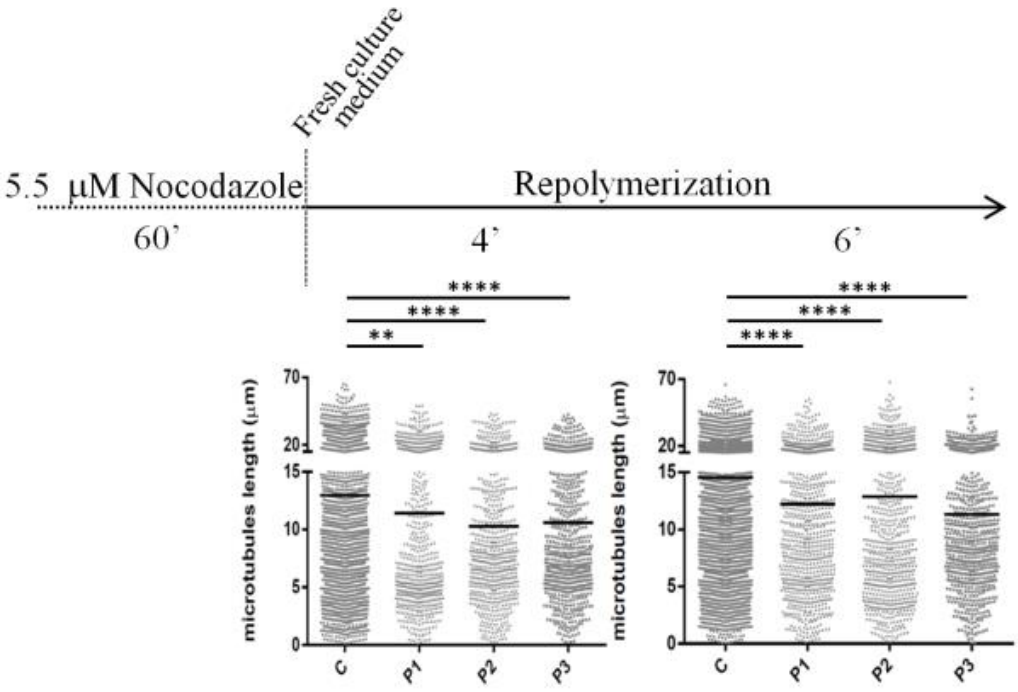

Figure S4. *TUBB4B* c.1172G>A and c.1171C>T mutations affect the rate of growth of patient fibroblast MTs after complete deploymerization with nocodazole. Fibroblasts were incubated for 60 min. in 5.5 µM nocodazole before fixation and further treatment and staining as described in Figure S2. The length of individual repolymerizing microtubules was measured from EB1 to the centrosome using Icy software and is plotted as a dot, with the mean distance represented by a horizontal line. Statistical analyses were carried out by analysis of variance (ANOVA) and the PLSD Fisher test. **: p-value <0.01; ****: p-value < 0.0001; n.s.: non-significant p-value ≥ 0.5.

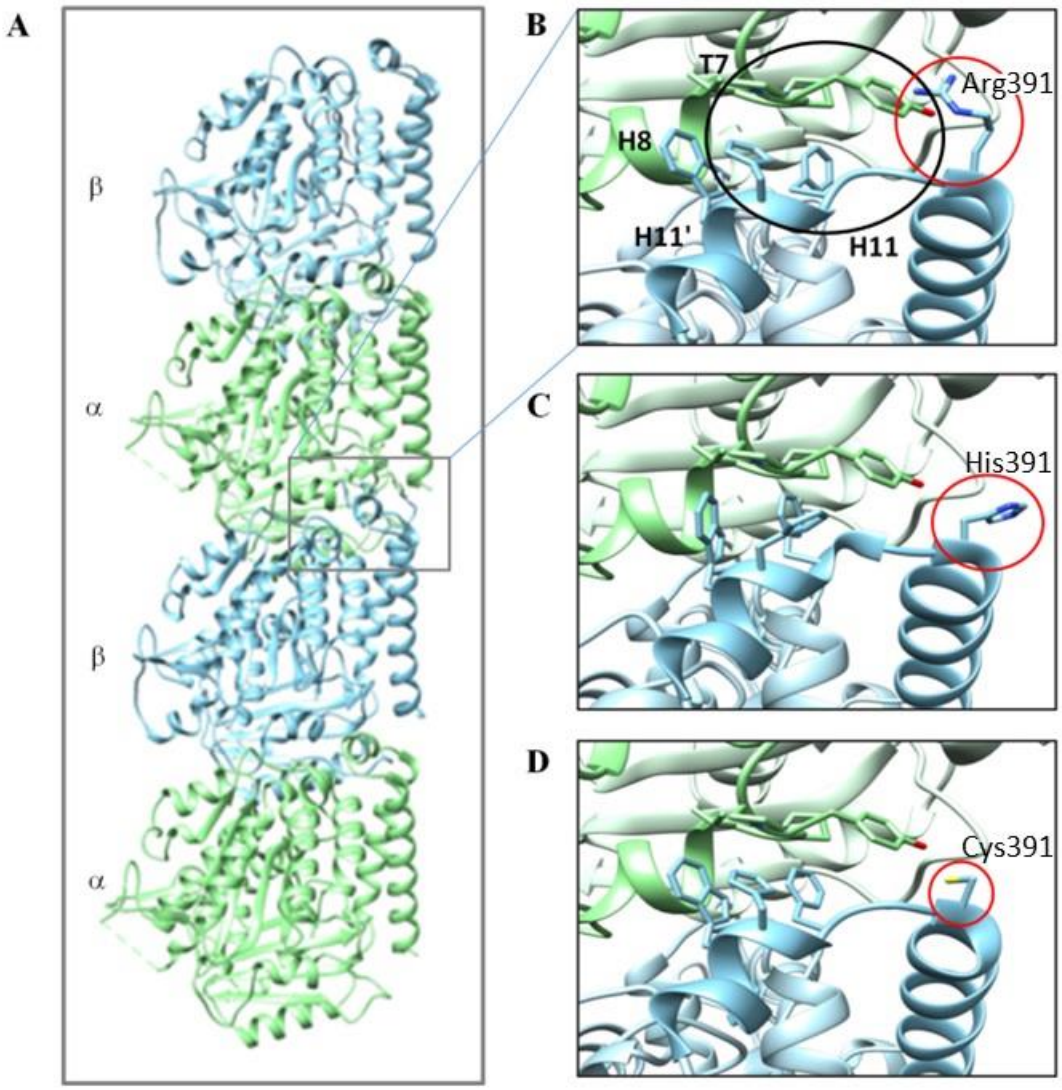

Figure S5. Predicted TUBB4B conformational changes induced by p.Arg391Cys and p.Arg391His substitutions. The structure of the end of the H11 helix in β-tubulin-bound α-tubulin (β-tubulin in blue, α-tubulin in green) is shown. The figures were generated with I-Tasser. Predicted models were aligned on the cryo-electron microscopy structure of a GDP-protofilament (GDP-K MT, EMD-6353, PDB: 3JAS) using UCSF Chimera software.[2-4]

(**A**) Overview of αβ-tubulin heterodimers within an assembled microtubule.

(**B**) The p.Arg391 residue at the end of helix H11 in β-tubulin contributes to a binding pocket that interacts with α-tubulin in the longitudinally adjacent heterodimer.

(**C, D**) The p.Arg391His (**C**) and p.Arg391Cys (**D**) substitutions were introduced to show their respective effects on the binding pocket.

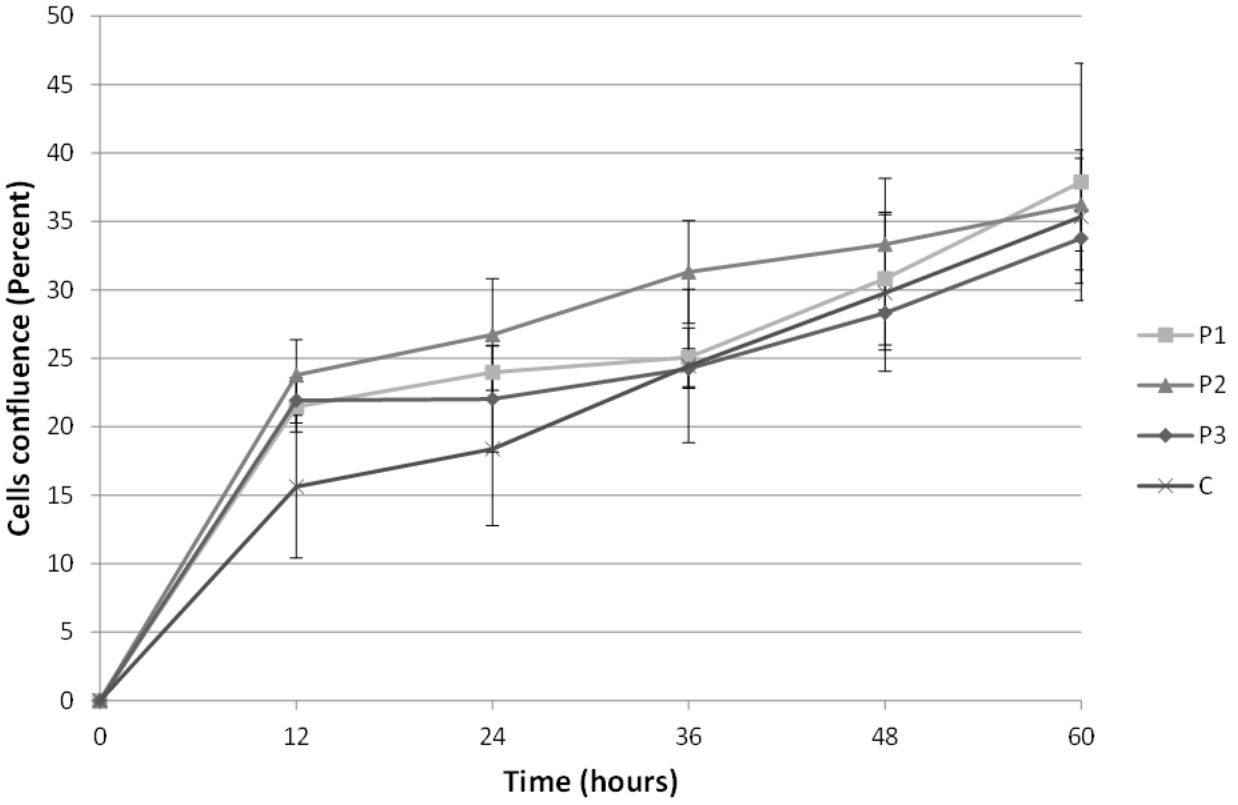

Figure S6. TUBB4B p.Arg391Cys and p.Arg391His substitutions do not affect fibroblast proliferation as determined by a live cell proliferation assay. A real time cell analyzer (RTCA) xCELLigence (ACEA Bioscience Inc., San Diego, CA) was used to monitor fibroblast cell proliferation based on impedance measurements. Cells (n= 1350 per well) were seeded in 96-well E-plates (ACEA Bioscience Inc.) contained in Opti-MEM Glutamax I medium (Life Technologies ThermoFisher Scientific) supplemented with 10% fetal bovine serum (Life Technologies ThermoFisher Scientific) and 1% streptomycin/penicillin (Life Technologies ThermoFisher Scientific). Variations in the impedance signal, expressed as cell index (CI), was recorded at 37 °C, 5% CO_2 every 12 hours for 5 days. CI were measured for each cell line and culture condition in triplicate. The cell doubling time (CDT) was determined in each well using RTCA software v1.2.1. The significance of CDT variations among samples was determined using a Mann-Whitney statistic test. Data are presented as mean ± SD.

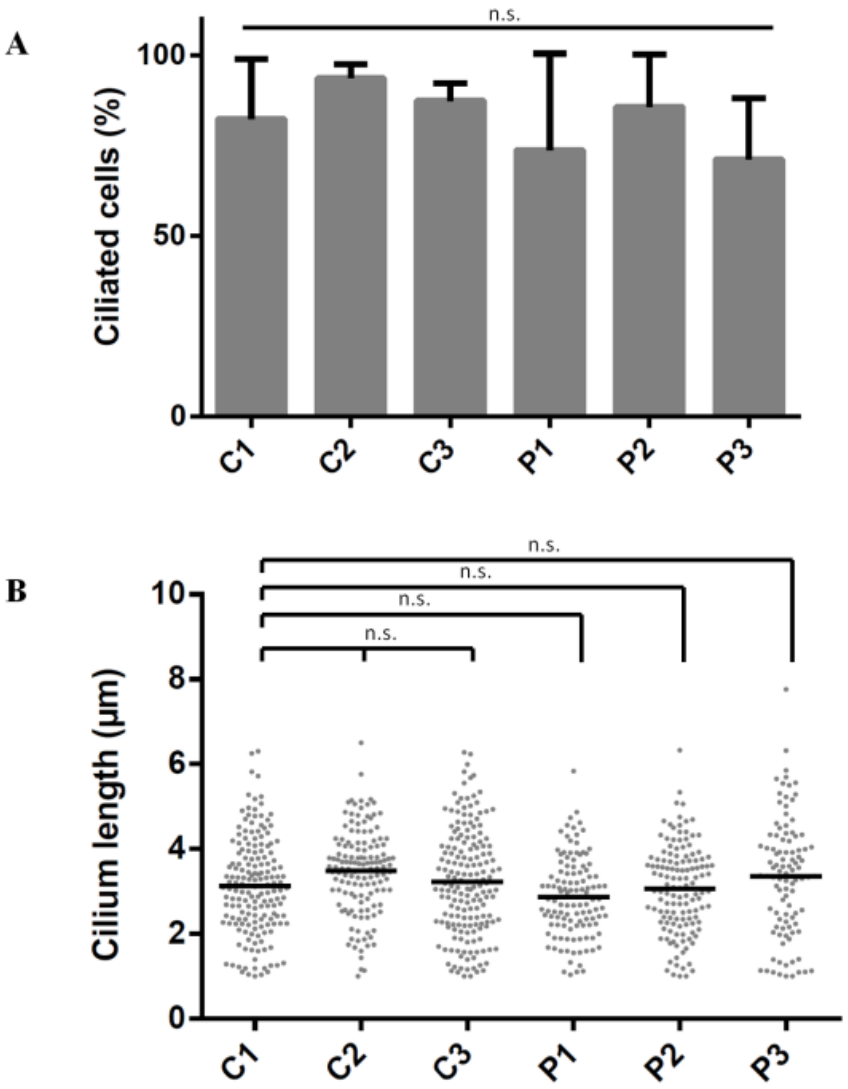

Figure S7. TUBB4B p.Arg391Cys and p.Arg391His substitutions do not affect fibroblast ciliogenesis. Immunofluorescence staining and cilia length measurements in cultured human fibroblasts from healthy (C1, C2, C3) and affected (P1, P2, P3) individuals were performed as described previously.[5-6]

(**A**) The proportion of fibroblasts containing a primary cilium was calculated by examining at least 100 cells in at least four fields from two independent experiments. Data are presented as mean ± SD.

(**B**) The length of individual primary cilia among > 100 ciliated cells from C1, C2, C3, P1, P2 and P3, respectively, is plotted as a dot, with the mean distance represented by a horizontal line. n.s.: non-significant $p \geq 0.5$.

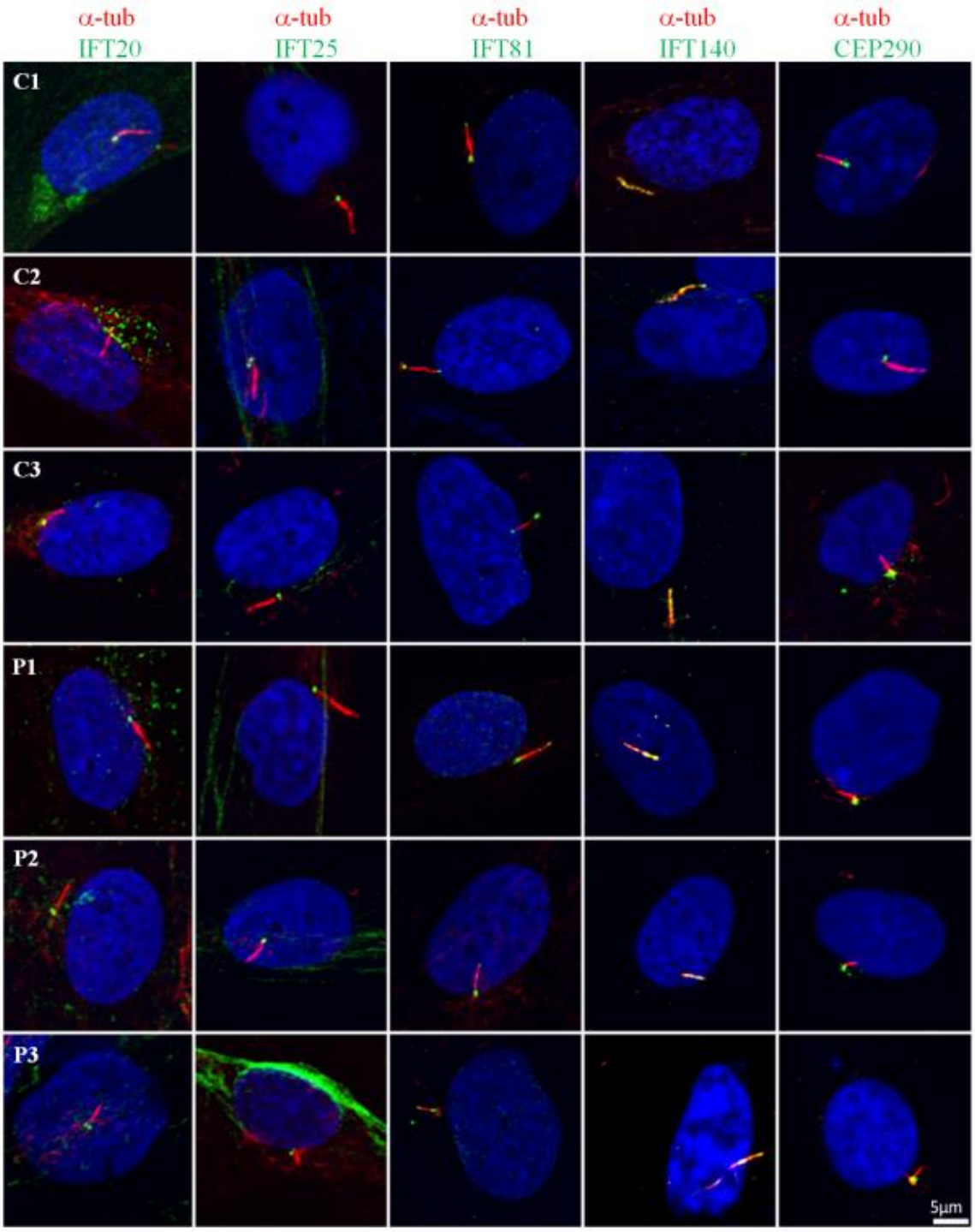

Figure S8. TUBB4B p.Arg391Cys and p.Arg391His substitutions do not affect the localization of the intraflagellar transport IFT20, IFT25, IFT81, IFT140 proteins or the centrosomal CEP290 protein in the fibroblasts of affected individuals. Immunofluorescence staining was performed in cultured human fibroblasts from healthy control (C1, C2, C3) and affected (P1, P2, P3) individuals as described previously.[5-6] Ciliary axonemes were stained using mouse monoclonal anti-acetylated α-tubulin (red). Ciliary signals obtained using antibodies to IFT20, IFT25, IFT81, IFT140 and CEP290 (green) did not show any significant difference among >20 ciliated control and mutant cells.

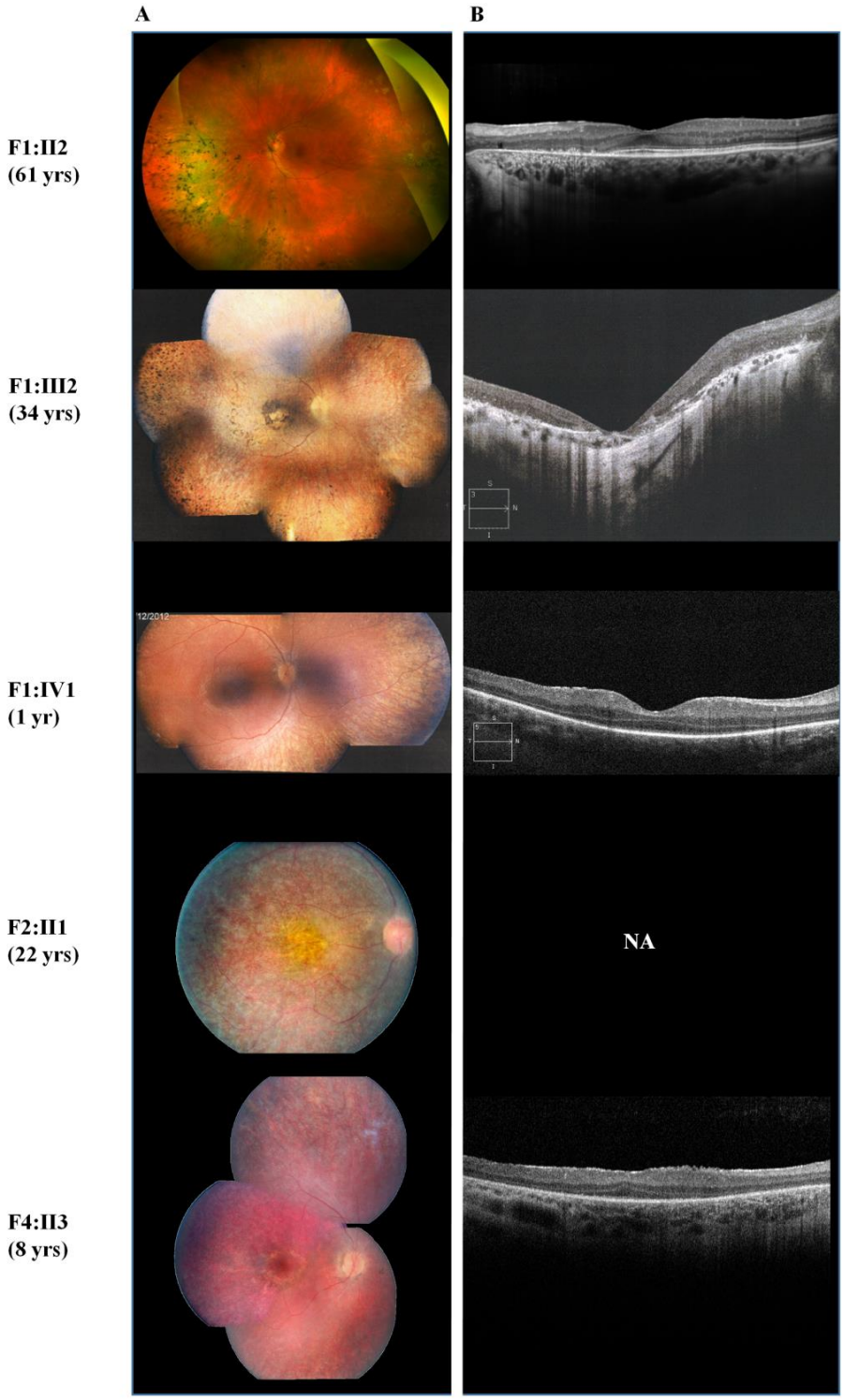

Figure S9. Representative fundus and optic coherence tomography (OCT) in individuals with TUBB4B substitutions affecting p.Arg391. (**A**) Right eye fundi showing thin retinal vessels, salt and pepper appearance of the posterior pole, yellowish peripheral retina with round pigmented spots at the fundus in F1:II2 and F1:III1 and macular reorganization in F1:II2. (**B**) Right eye spectral domain OCT revealing marked alteration of the retinal structure in F1:II2 and relatively preserved outer retina in the foveal and parafoveal area but not outside the central region in F1:III1 and F4:II3.

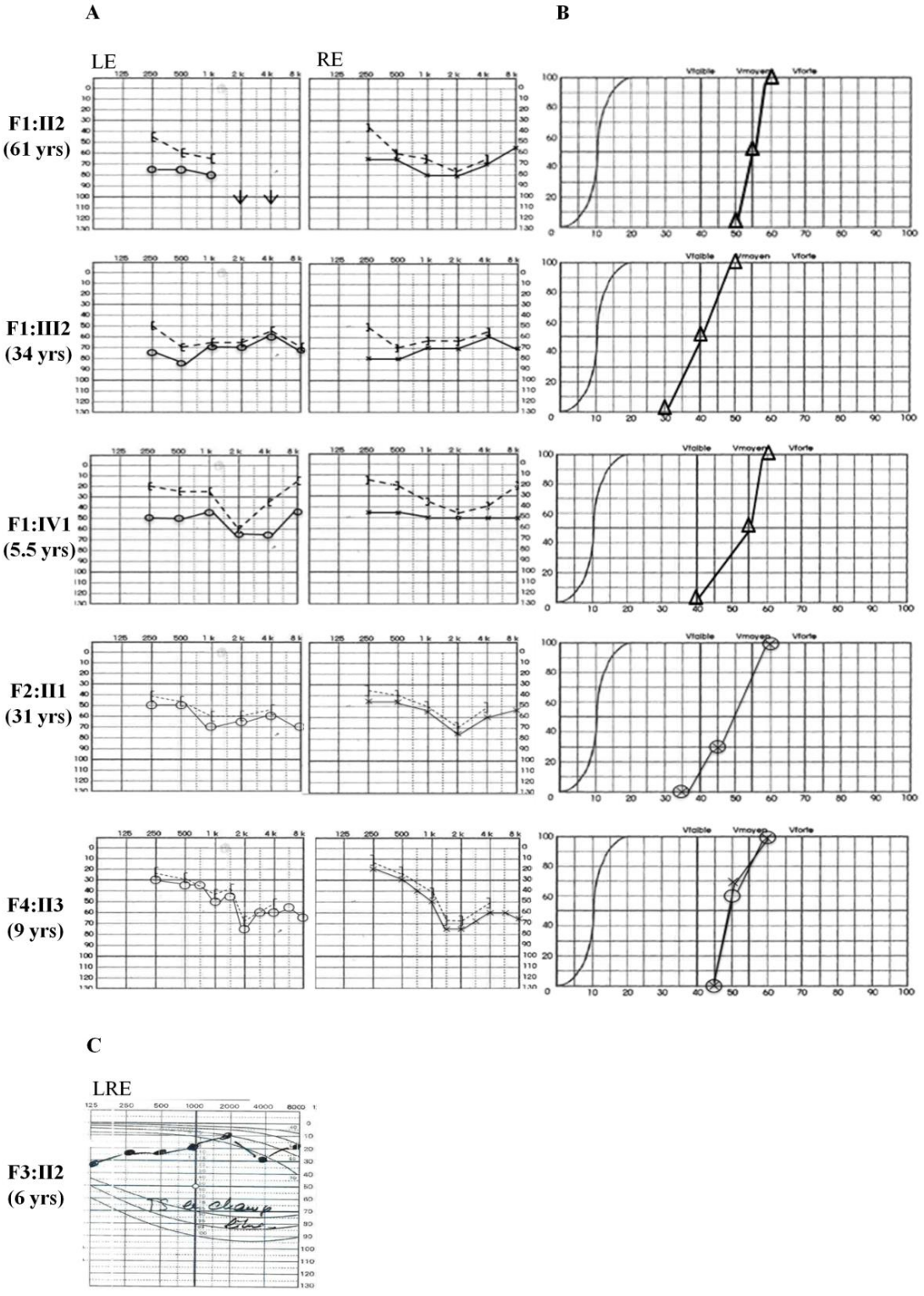

Figure S10. Representative auditory defects in individuals with TUBB4B substitutions affecting p.Arg391. (**A**) Pure Tone Audiometry using Air Sound conduction (circles) and Bone Sound conduction (crosses). (**B**) Speech Audiometry. (**C**) Free field Air conduction Thresholds. LE: Left ear, RE: Right ear, LRE: left and right ears. (yrs: years).

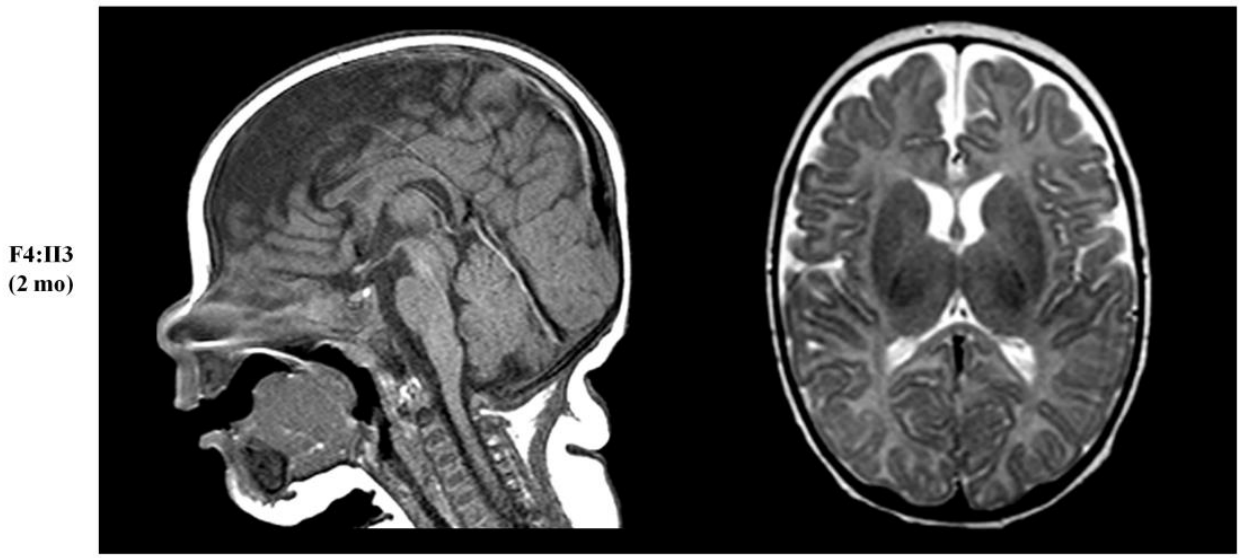

Figure S11. Brain MRI. Sagittal T1 weighted MRI (Left panel) and Right Axial T2 weighted image (right panel) showing normal cortical gyration and brain anatomy. The age of the affected individual at examination is given in parentheses (mo: months).

A

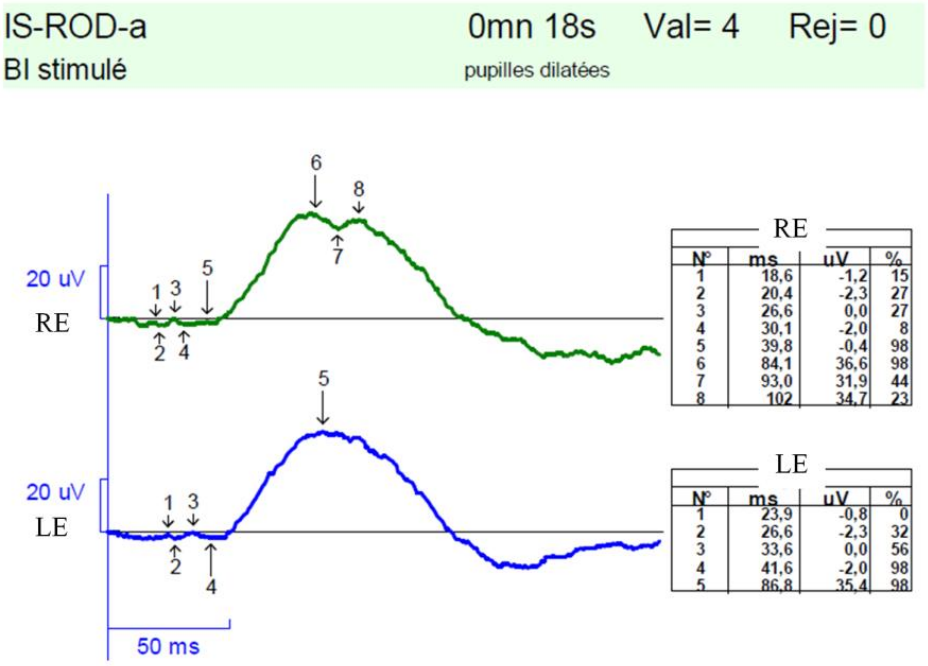

B

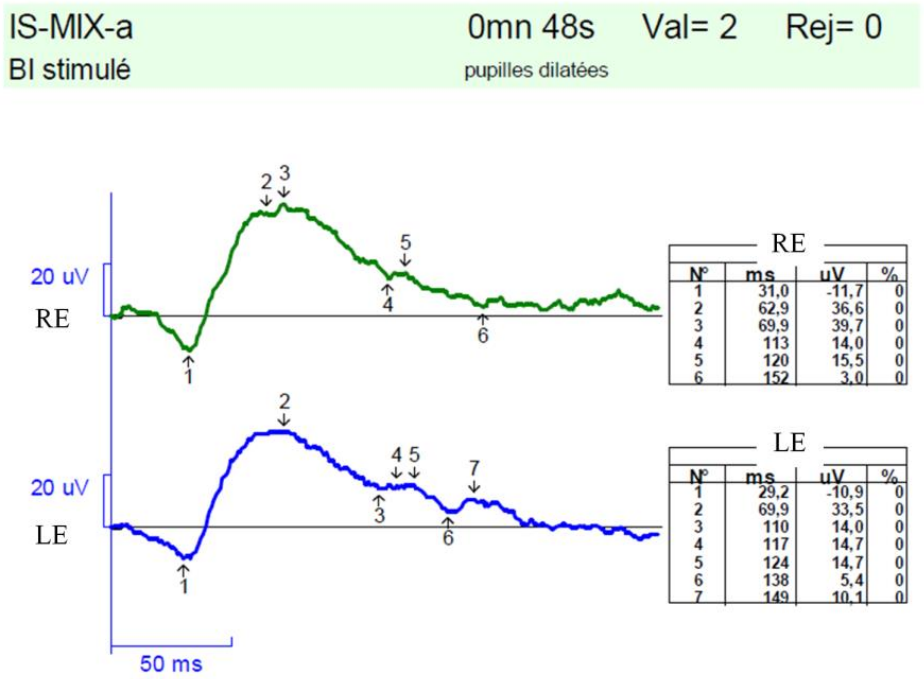

Figure S12. Electroretinogram responses of the right and left eyes (RE and LE, respectively) of subject F1:II.2 carrying the c.1172G>A mutation on 29% of *TUBB4B* alleles. (A) Flash-ERG ROD response: amplitude and morphology of waves are normal. **(B)** Flash-ERG Mixed response: amplitude and morphology of waves are normal.

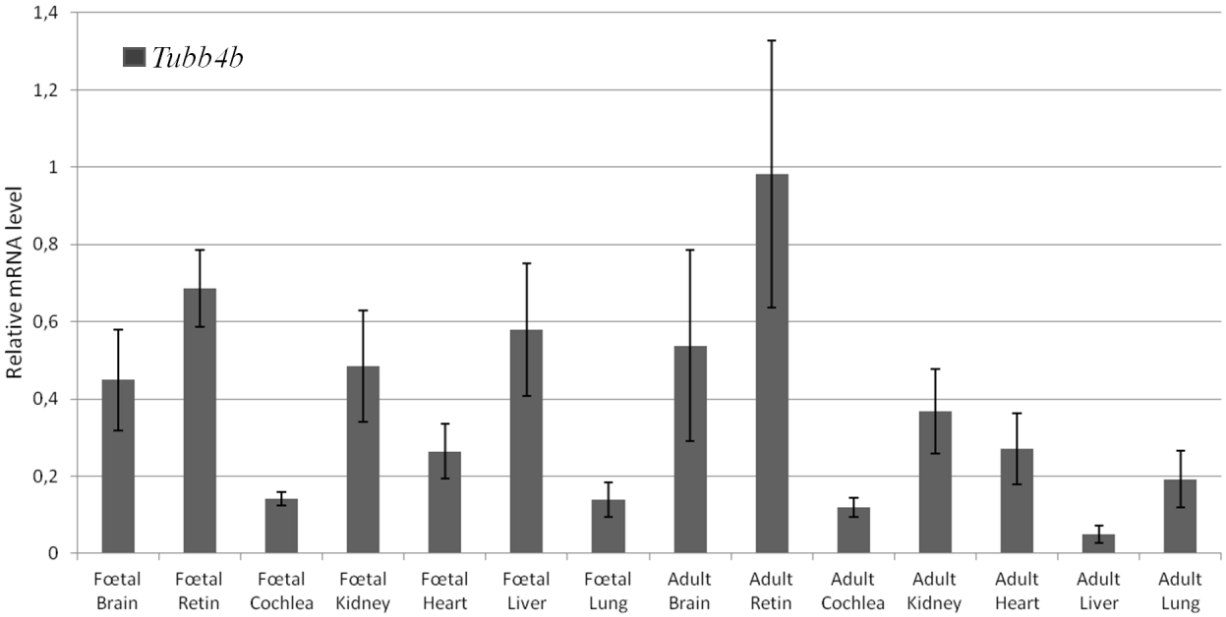

Figure S13. RTqPCR expression analysis of *tubb4b* mRNA in embryonic and adult mouse tissues showing high retinal but not cochlear *tubb4b* expression. *tubb4b* mRNA was amplified as a 64 bp fragment using exonic primers: (forward, 5'-3') cgaagccaccggtggcaa and (reverse, 5'-3') catggtgccgggctccaa. *B2m*, *Hprt1*, *Rplp0* mRNAs and the *Alb* gene primers were used to normalize the data and to control for the absence of contamination of cDNAs by genomic DNA. Primer sequences are available elsewhere.[7] Data are presented as mean ± SEM from three independent experiments.

Table S1. Whole exome resequencing coverage and read-depth.

		Coverage		
Family	**Individual**	**Mean**	**15X**	**30X**
1	II1	103.2	98.7	94.2
	II2	188.4	96.7	96
	III2	172.9	99.4	98.4
	IV1	155.1	96.8	95.7
2	I1	123	96.6	94.8
	I2	141.1	96.6	95.4
	II1	129.8	96.7	95.3
3	I1	128.8	96.6	95.1
	I2	132.4	96.5	95.1
	II2	178.3	99.3	98.3
4	I1	156.8	98.6	97.1
	I2	189.6	98.5	97.5
	II3	211.5	98.8	98

Table S2. Whole exome resequencing data. Exhaustive list of rare SNVs/indels and *de novo* and recessive variants identified in the four families. The deleterious effect of variants was assessed using the Alamut Mutation Interpretation software which uses Polyphen 2, SIFT, Mutation Taster, GVGD, SpliceSiteFinder-like, MaxEntScan, NNSPLICE and/or Human Splicing Finder. MAF: minor allele frequency.

Provided as an excel file

Table S3. PCR-based deep sequencing of *TUBB4B* exon 4 identifies mosaicism and *de novo* mutations. The quantification of the ratio of mutant to wild-type sequence reads is presented for all affected individuals and their parents.

Family	Individual	Total number of reads	Number of wild-type reads	Number of mutant reads	Percentage of mutant alleles
F1	II-1	2000	1991 G	5 A	0.25
	II-2	1956	1386 G	570 A	29.1
	III-1	2087	2087 G	0 A	0
	III-2	2215	1147 G	1063 A	47.9
F2	I-1	1712	1712 G	0 A	0
	I-2	1891	1644 G	245 A	12.9
F3	I-1	1997	1995 G	2 A	0.1
	I-2	2258	2254 G	3 A	0.13
F4	I-1	2225	2223 C	2 T	0.09
	I-2	1998	1995 C	2 T	0.1

Table S4. Oligonucleotides used for PCR and Sanger sequencing.

Exon	Orientation	Sequence (5'-3')
1	*forward*	ggcaaggccaatcaaacgag
	reverse	tgctcatcgctgatcacctc
2	*forward*	caaattcggcgccaaggtaa
	reverse	cacggctcaccgaaaacg
3	*forward*	gcgtcccttgtagttttggga
	reverse	gagcagccccttgacctttg
4	*forward*	gtggtcagctcacaccatgt
	reverse	aggaatgggcaaagcgaaac

References.

1. Gerard, X., Perrault, I., Hanein, S., Silva, E., Bigot, K., Defoort-Dellhemmes, S., Rio, M., Munnich, A., Scherman, D., Kaplan, J., Kichler, A., Rozet, J.M. (2012). AON-mediated Exon Skipping Restores Ciliation in Fibroblasts Harboring the Common Leber Congenital Amaurosis CEP290 Mutation. Mol. Ther. Nucleic Acids. *1*, e29.
2. Pettersen, E.F., Goddard, T.D., Huang, C.C., Couch, G.S., Greenblatt, D.M., Meng, E.C., Ferrin, T.E. (2004). UCSF Chimera--a visualization system for exploratory research and analysis. J. Comput. Chem. *25*, 1605-12.
3. Yang, J., Yan, R., Roy, A., Xu, D., Poisson, J., Zhang, Y. (2015). The I-TASSER Suite: protein structure and function prediction. Nat. Methods *12*, 7-8.
4. Zhang, R., Alushin, G.M., Brown, A., Nogales, E. (2015). Mechanistic Origin of Microtubule Dynamic Instability and Its Modulation by EB Proteins. Cell *162*, 849-59.
5. Perrault, I., Halbritter, J., Porath, J.D., Gérard, X., Braun, D.A., Gee, H.Y., Fathy, H.M., Saunier, S., Cormier-Daire, V., Thomas, S., Attié-Bitach, T., Boddaert, N., Taschner, M., Schueler, M., Lorentzen, E., Lifton, R.P., Lawson, J.A., Garfa-Traore, M., Otto, E.A., Bastin, P., Caillaud, C., Kaplan, J., Rozet, J.M., Hildebrandt, F. (2015). IFT81, encoding an IFT-B core protein, as a very rare cause of a ciliopathy phenotype. J. Med. Genet. *52*, 657-65.
6. Perrault, I., Saunier, S., Hanein, S., Filhol, E., Bizet, A.A., Collins, F., Salih, M.A., Gerber, S., Delphin, N., Bigot, K., Orssaud, C., Silva, E., Baudouin, V., Oud, M.M., Shannon, N., Le Merrer, M., Roche, O., Pietrement, C., Goumid, J., Baumann, C., Bole-Feysot, C., Nitschke, P., Zahrate, M., Beales, P., Arts, H.H., Munnich, A., Kaplan, J., Antignac, C., Cormier-Daire, V., Rozet, J.M. (2012). Mainzer-Saldino syndrome is a ciliopathy caused by IFT140 mutations. Am. J. Hum. Genet. *90*, 864-70.
7. Gerard X, Perrault I, Munnich A, Kaplan J, Rozet JM. (2015). Intravitreal Injection of Splice-switching Oligonucleotides to Manipulate Splicing in Retinal Cells. Mol. Ther. Nucleic Acids. *4*, e250.